Available online at www.sciencedirect.com
SCIENCE DIRECT®
Journal of Sound and Vibration 269 (2004) 273–294
JOURNAL OF SOUND AND VIBRATION
www.elsevier.com/locate/jsvi

Comparative analysis of actuator concepts for active gear pair vibration control ☆

Yuan H. Guan[a], Mingfeng Li[b], Teik C. Lim[b,*], W. Steve Shepard Jr[a]

[a] *Department of Mechanical Engineering, University of Alabama, 290 Hardaway Hall, Box 870276, Tuscaloosa, AL 35487, USA*

[b] *Mechanical, Industrial and Nuclear Engineering, University of Cincinnati, 624 Rhodes Hall, P.O. Box 210072, Cincinnati, OH 45221, USA*

Received 11 March 2002; accepted 14 December 2002

Abstract

Four actuation concepts for the active suppression of gearbox housing mesh frequency vibrations due to transmission error excitation from the gear pair system are modelled and compared by computing the required actuation forces and amplifier power spectra. The proposed designs studied consist of (1) active inertial actuators positioned tangentially on the gear body to produce a pair of reactive force and moment, (2) semi-active gear–shaft torsional coupling to provide tuned vibration isolation and suppression, (3) active bearing vibration control to reduce vibration transmissibility, and (4) active shaft transverse vibration control to suppress/tune gearbox casing or shaft response. Numerical simulations that incorporate a transmission error term as the primary excitation are performed using a finite element model of the geared rotor system (dynamic plant) constructed from beam and lumped mass/stiffness elements. Several key comparison criteria including the required actuation effort, control robustness and implementation cost are examined, and the advantages and disadvantages of each concept are discussed. Based on the simulated data, the active shaft transverse vibration control scheme is identified as the most suitable approach for this application.

1. Introduction

Although numerous applications of smart material systems for vibration control exist [1–4], many of these applications only deal with controlling of the response from the first few resonant

☆ Part of this paper was presented at the SPIE Ninth Annual International Symposium on Smart Structures and Materials, San Diego, CA, March 2002.

*Corresponding author. Tel.: +1-513-556-4450; fax: +1-513-556-3390.
E-mail address: teik.lim@uc.edu (T.C. Lim).

0022-460X/03/$ - see front matter
doi:10.1016/S0022-460X(03)00072-5

modes of simple structures such as beams and plates. Moreover, these resonance frequencies are often less than a few hundred Hertz. Very few applications involve the control of complex machinery such as a gearbox system. The lack of application in more industrial-relevant systems is likely due to several reasons. For many machinery structures, the modal densities are often quite high in the mid- and high-frequency ranges. In these frequency ranges, the individual modes can be difficult to identify and control. Moreover, these higher-order modes are typically quite complex and thus difficult to attenuate. In the case of the gearbox system, though, its response tends to be dominated by the mesh frequency (given by the product of the number of the teeth and shaft speed) and its harmonics that span over a wide frequency range. The gearbox system can exhibit non-linear and time-varying characteristics especially under small load, light damping and high rotation speed conditions [5]. Nevertheless, when the transmitted load and damping levels are sufficiently high, and the rotation speed is low enough such that the operating mesh frequency is significantly below the fundamental gear pair resonance point, the gearbox system can be considered to be linear if backlash is ignored. The discrete nature of the spectral peaks makes this complex system a potentially suitable candidate for active control using smart material systems. Recent active vibration and acoustic noise control studies that involve gears are briefly reviewed next.

In 1999, Rebbechi et al. [6] presented a method for performing active control of a gearbox by attempting to actively isolate the vibration between the shaft and housing via a pair of magnetostrictive actuators mounted at one of the support bearing locations. It was demonstrated that the housing vibration and acoustic noise response of the fundamental gear mesh frequency and its first two harmonics could be simultaneously reduced. A reduction of 20–28 dB was reportedly achieved at the fundamental frequency, while reductions of only 2–10 dB were achieved at the harmonics. More recently, Chen and Brennan [7] proposed a control scheme that used three magnetostrictive actuators mounted directly on the gear to produce circumferential forces for suppressing the torsional vibrations. The experimental results showed about 7 dB of reduction in gear angular vibrations at the tooth meshing frequencies between 150 and 350 Hz. Other than these studies, no other recent work on the active vibration control of internal gearbox components is found in the public domain literature. There are several related studies that concentrated on active vibration control applied to the structural support system outside of the gearbox [8–10], including attaching inertial actuators to the gearbox strut.

In the limited number of investigations on active vibration control of a gearbox system, no comparison of different actuation approaches and the resulting performance gains has been performed. Since the actuator is one of the primary elements and its set-up may significantly affect the performance of the active vibration control system, it is highly desirable to be able to identify an effective configuration. In this paper, a comparative analysis is presented for the dynamic performances of four potentially feasible actuation concepts used to suppress housing vibration in a gear pair system. The objective of this computational study is to determine the most promising actuation method from these four approaches for future hardware development. First, a description of the gear pair system of interest and its corresponding finite element (FE) model, which is constructed using beam, lumped mass, and stiffness elements, is given. Using this model, the transfer functions between the actuation and sensor positions, which are needed for the active control simulation work, are determined. Then, the proposed actuation concepts are discussed in detail along with the methods for determining the required actuation forces and driving power

requirements. The sensitivity of these actuation concepts to measurement noise is also examined. Finally, several comparison criteria are given, and the advantages and disadvantages of each concept are discussed. The results of this comparison are then used to determine the most suitable active vibration control approach for the particular gearbox system under consideration. To generalize the conclusions further, selected parametric studies are also performed. As for the studies described above, the gearbox system is considered to be linear and backlash is ignored.

2. Gear pair model

A cross-section of the single-stage geared rotor system considered in this study is shown in Fig. 1. This system consists of a pair of thin spur gears, an AC electric drive motor, a DC load dynamometer, a torque transducer, three shaft-to-shaft couplings, and a series of driver and driven shaft segments. The system parameters are listed in Table 1. A physical laboratory set-up of this gearbox has been developed for use in future active vibration control implementation. The main vibration and acoustic noise source of interest to this study is the gear transmission error at the mesh. It is commonly known that the transmission error excitation interacts with the system dynamic characteristics to generate a dynamic mesh force that in turn excites the rest of gearbox structure. The resulting vibrational energy is transmitted through the shafts and bearings and into the housing where some of this energy is ultimately radiated as high-frequency gear whine noise that can be very annoying. Since the frequency of the gear tones are significantly higher than the shaft rotational speed, they can be easily monitored and identified. This frequency identification ability is essential for the active vibration control implementation considered here.

A dynamic FE model of the gear pair system is first developed for use in examining the four proposed actuation concepts. The model, which is constructed from beam elements and lumped masses and springs, provides an analytical representation of the critical gear rotational and translational vibration characteristics. The shafts are assumed flexible in the transverse and torsional directions. The longitudinal degree of freedom is neglected since no significant axial

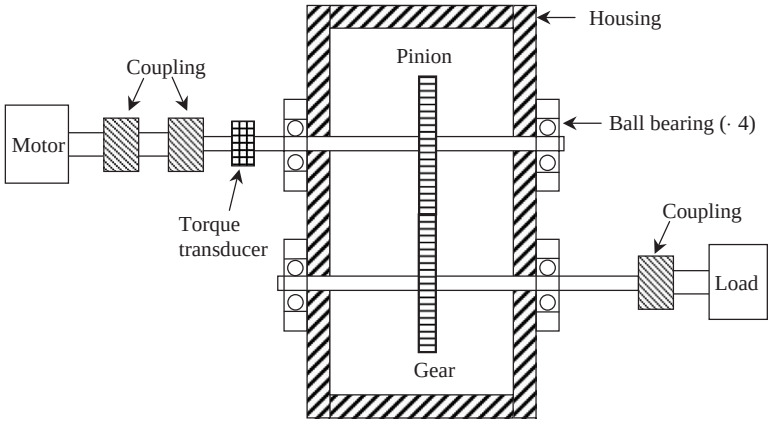

Fig. 1. A single-stage geared rotor system example.

Table 1
Geared rotor system design parameters

Parameter description	Numerical values (units)
Driven shaft length, L_{S1}	0.216 m
Driving shaft length, L_{S2}	0.213 m
Bearing stiffness, K_{bx}	2×10^7 N/m
Gear face width, W_f	9.53×10^{-3} m
Coupling mass , m_c	0.313 kg
Coupling inertia, I_c	5.05×10^{-5} kg m^2
Large shaft length, L_{ls}	5.08×10^{-2} m
Gear and pinion mass, m_g, m_p	0.53 kg
Gear and pinion radius, R_g, R_p	3.81×10^{-2} m
Gear mesh stiffness, K_m	1.48×10^8 N/m
Housing mass, m_h	100 kg
Motor inertia, I_m	3.45×10^{-3} kg m^2
Load inertia, I_d	17.65×10^{-3} kg m^2
Shaft radius, R_s	4.76×10^{-3} m
Large shaft radius, R_{ls}	9.5×10^{-3} m

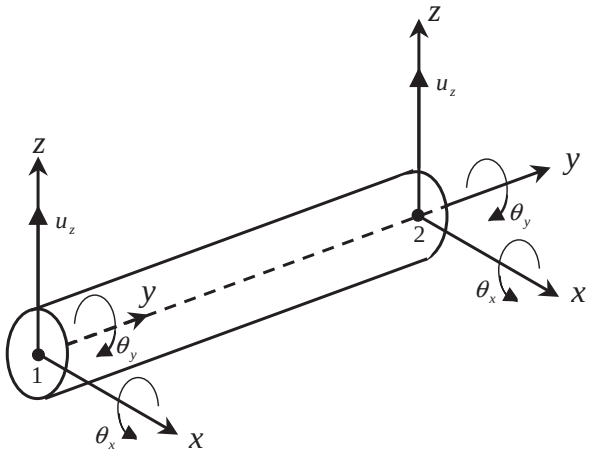

Fig. 2. A 2-noded beam element with transverse u_z parallel to the gear mesh line-of-action, bending rotation θ_x and torsion θ_y co-ordinates used to construct the input and output shaft models. The nodes are labelled as points 1 and 2.

excitation is expected from the spur gears and to avoid unnecessary complexity in the analysis [11]. Moreover, the natural frequency associated with the longitudinal vibration is much higher than the frequency range of interest. Accordingly, each nodal point on the discretized shaft is only defined by three degrees of freedom (d.o.f.) that include transverse, bending rotation and torsion co-ordinates as shown in Fig. 2. The beam element stiffness matrix formulation can be

shown to be

$$\mathbf{K}^e_{beam} = \begin{bmatrix} 12K_1 & 6K_1L & 0 & -12K_1 & 6K_1L & 0 \\ 6K_1L & 4K_1L^2 & 0 & -6K_1L & 2K_1L^2 & 0 \\ 0 & 0 & K_s & 0 & 0 & -K_s \\ -12K_1 & -6K_1L & 0 & 12K_1 & -6K_1L & 0 \\ 6K_1L & 2K_1L^2 & 0 & -6K_1L & 4K_1L^2 & 0 \\ 0 & 0 & -K_s & 0 & 0 & K_s \end{bmatrix}, \tag{1}$$

where L is the element length, $K_s = GJ/L$, $K_1 = EI/L^3$, E is the modulus of elasticity, I and J are the area and polar moments of inertia, respectively, and G is the shear modulus. The corresponding mass matrix is

$$\mathbf{M}^e_{beam} = \frac{m}{420}\begin{bmatrix} 156 & 22L & 0 & 54 & -13L & 0 \\ 22L & 4L^2 & 0 & 13L & -3L^2 & 0 \\ 0 & 0 & 70R^2 & 0 & 0 & 35R^2 \\ 54 & 13L & 0 & 156 & -22L & 0 \\ -13L & -3L^2 & 0 & -22L & 4L^2 & 0 \\ 0 & 0 & 35R^2 & 0 & 0 & 70R^2 \end{bmatrix}, \tag{2}$$

where m is the element mass and R is the shaft radius. These matrices correspond to the co-ordinate vector $\{u_{z1}, \theta_{x1}, \theta_{y1}, u_{z2}, \theta_{x2}, \theta_{y2}\}^{\mathrm{T}}$, where the numeric subscript represents the corresponding node in Fig. 2.

The gear mesh kinematics is modelled using a concept originally proposed by Tuplin [12], which has been widely used by many gear researchers [13–15]. The linear time-invariant model consists of an infinitesimal spring–damper element positioned in series with the loaded static transmission error excitation $e(t)$ at the mesh point as shown in Fig. 3. The mesh model couples the translational co-ordinates of the gear and pinion centroids along the tooth load line-of-action. Additionally, the bending rotation and torsion co-ordinates of the gears are considered, which match exactly to the corresponding shaft degrees of freedom. However, the direct coupling between the gear bending rotation and the other two gear co-ordinates is assumed negligible when formulating the mesh model because of the horizontally straight spur gear tooth arrangement and

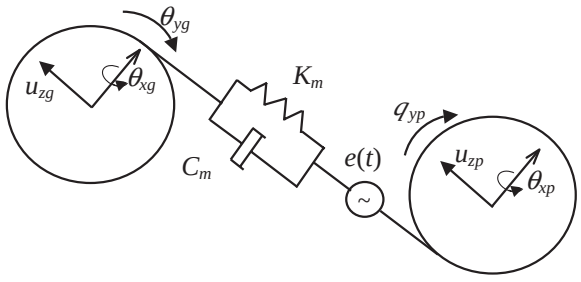

Fig. 3. An infinitesimal spring–damper gear mesh model.

the fact that the shaft geometries are nearly symmetric with respect to the gear and pinion positions. The gear bending rotation and transverse co-ordinates are in fact coupled directly through the beam element stiffness, which is in turn coupled to the torsion co-ordinate via the mesh stiffness. This is because the nodes representing the pinion and gear coincide with the nodes of the respective beam elements at the position of gear bodies. The lumped parameter gear pair model that incorporates the discrete masses and inertias of the gear bodies and its spring stiffness of the meshing kinematics are added to the beam parameters at the relevant nodal co-ordinates. In our analysis, the gear mesh stiffness is specified to be constant [16]. Secondary effects including gear backlash, gear run-out or eccentricity, gyroscopic term and frictional force between mating teeth are ignored since the primary focus is on the comparison of the performance of various actuation concepts for controlling gear mesh frequency response due to transmission error excitation under loaded conditions. Hence, the instantaneous position of each gear body is defined by one translational and two rotational co-ordinates expressed as u_z, θ_x and θ_y. For the combined gear–pinion system, the position vector is $\{u_{zg}, \theta_{xg}, \theta_{yg}, u_{zp}, \theta_{xp}, \theta_{yp}\}$, where the subscripts g and p represent gear and pinion, respectively. The corresponding mesh stiffness and gear mass matrices are

$$\mathbf{K}^e_{mesh} = \begin{bmatrix} K_m & 0 & -K_m R_g & -K_m & 0 & -K_m R_p \\ 0 & 0 & 0 & 0 & 0 & 0 \\ -K_m R_g & 0 & K_m R_g^2 & K_m R_g & 0 & K_m R_g R_p \\ -K_m & 0 & K_m R_g & K_m & 0 & K_m R_p \\ 0 & 0 & 0 & 0 & 0 & 0 \\ -K_m R_p & 0 & K_m R_p R_g & K_m R_p & 0 & K_m R_p^2 \end{bmatrix}, \tag{3}$$

$$\mathbf{M}^e_{mesh} = \begin{bmatrix} m_g & 0 & 0 & 0 & 0 & 0 \\ 0 & I_{xg} & 0 & 0 & 0 & 0 \\ 0 & 0 & I_{yg} & 0 & 0 & 0 \\ 0 & 0 & 0 & m_p & 0 & 0 \\ 0 & 0 & 0 & 0 & I_{xp} & 0 \\ 0 & 0 & 0 & 0 & 0 & I_{yp} \end{bmatrix}, \tag{4}$$

where K_m is the gear mesh stiffness, and (R_g, R_p), (m_g, m_p), (I_{xg}, I_{xp}), and (I_{yg}, I_{yp}) are the radii, masses and mass moment of inertias of the gear and the pinion about the x and y directions, respectively. Note that the above formulation is quite similar to the one proposed by Lim and Singh [17]. Here, the model has been extended to include bending rotation.

Both the motor and load components are also modelled as lumped mass moment of inertias, while the bearings are formulated using lumped spring elements having the ability to resist motion in the transverse (parallel to the line-of-action) and bending rotation directions. The housing structure is represented as a 1-d.o.f. rigid body (lumped mass element) connected to the gear train at the four bearing locations via a set of bearing stiffnesses. This rigid body housing approximation does not pose a significant limitation to the simulation work, as the focus of this study is to control the overall housing vibrations via the internal gear–shaft dynamics. In fact,

this simplified housing model eases simulation efforts. The assembled system model contains 39 finite elements including 10 lumped masses, four lumped springs, 24 beam elements and a single gear mesh stiffness element. The model has twenty-four 3-d.o.f. nodes and three 1-d.o.f. nodes for the motor, load and housing. This gives a total of $N=75$ d.o.f.s for the complete system co-ordinate set. Note that the treatment of the motor, load and bearing components in the model is similar to the approach used by Ozguven [18]. Since the shafts in the single-stage geared rotor system are relatively thin and compliant, their transversal and bending motions are included as well as the torsion co-ordinate. As the result, there are more d.o.f.s in the present dynamic model than the 6 d.o.f.s formulated by Ozguven [18]. Since the work presented here is primarily interested in active vibration control of a gearbox with sufficiently high load and damping levels, negligible backlash and low operating mesh frequencies, only a linear system behavior is considered here unlike the non-linear dynamic study performed by Ozguven [18].

The system mass $\mathbf{M}$ and stiffness $\mathbf{K}$ matrices, each of dimensions $N \times N$, can then be used to form the classical governing equation of dynamic motion expressed as

$$\mathbf{M}\ddot{\mathbf{X}} + \mathbf{C}\dot{\mathbf{X}} + \mathbf{K}\mathbf{X} = \mathbf{F}, \tag{5}$$

where $\mathbf{X}$ is the response vector, $\mathbf{F}$ is the forcing vector containing the transmission error term, $\mathbf{C}$ is the damping matrix assumed to be equivalent to the typical 5% uniform modal damping observed for gearing systems, and $\dot{\mathbf{X}}$ and $\ddot{\mathbf{X}}$ signify the first and second time derivatives of $\mathbf{X}$, respectively. Here, $\mathbf{M}$ and $\mathbf{K}$ are the summations of the expanded version of each element matrix derived using a standard FE formulation [11]. Note that Eq. (5) is linear and its coefficient matrices are time-invariant. An output vector, $\mathbf{Y} = \mathbf{D}\mathbf{X}$, is defined for a subset of the n response co-ordinates of interest, where $\mathbf{D}$ is the output coefficient matrix of dimension $n \times N$. Applying the theory of normal modes to Eq. (5), $\mathbf{X} = \mathbf{\Phi}\mathbf{Q}$ can be used to transform the representation from physical co-ordinates $\mathbf{X}$ into modal co-ordinates $\mathbf{Q} = \{q_1 \; q_2 \; \cdots q_N\}^{\mathrm{T}}$. Here, $\mathbf{\Phi}$ consists of the mass normalized mode shapes (eigenvectors) where $\mathbf{\Phi}^{\mathrm{T}}\mathbf{M}\mathbf{\Phi} = \mathbf{I}$ resulting in the identity matrix. The resulting dynamical equations in terms of these uncoupled modal co-ordinates are

$$\begin{Bmatrix} \dot{q}_1 \\ \ddot{q}_1 \\ \dot{q}_2 \\ \ddot{q}_2 \\ \cdots \end{Bmatrix} = \begin{bmatrix} 0 & 1 & 0 & 0 & \cdots \\ -\omega_1^2 & -2\zeta_1\omega_1 & 0 & 0 & \cdots \\ 0 & 0 & 0 & 1 & \cdots \\ 0 & 0 & -\omega_2^2 & -2\zeta_2\omega_2 & \cdots \\ \cdots & \cdots & \cdots & \cdots & \cdots \end{bmatrix} \begin{Bmatrix} q_1 \\ \dot{q}_1 \\ q_2 \\ \dot{q}_2 \\ \cdots \end{Bmatrix} + \mathbf{\Phi}^{\mathrm{T}} \begin{Bmatrix} 0 \\ F_1 \\ 0 \\ F_2 \\ \cdots \end{Bmatrix}, \tag{6}$$

where F_j ($j=1,2,\ldots,N$) is the element of the physical force vector $\mathbf{F}$, ω_i is the ith natural frequency, and ζ_i is the corresponding modal damping coefficient. In terms of the modal co-ordinates, the output vector is

$$\mathbf{Y} = \mathbf{D}\mathbf{\Phi}\mathbf{Q}. \tag{7}$$

Solving Eq. (6) for q_i and transforming them back into the physical co-ordinates yields the output response of interest. Accordingly, the transfer function between any kth reference co-ordinate

(forcing) and any jth physical response point is

$$H_{jk} = \frac{x_j}{F_k} = \sum_{i=1}^{N} \frac{\phi_{ji}\phi_{ki}}{s^2 + 2\zeta_i\omega_i s + \omega_i^2}, \tag{8}$$

where s is the Laplace variable. This FE model and the corresponding transfer function results derived above are employed in the subsequent active vibration control simulations to examine the true capabilities and limitations of the four proposed actuation concepts to minimize the gear housing vibration response.

3. Actuation concepts

The proposed four active vibration control concepts for suppressing the housing response as mentioned earlier include: (1) active inertial actuators positioned tangentially on the gear body, (2) semi-active gear–shaft torsional isolation coupling, (3) direct active bearing vibration control, and (4) active shaft transverse vibration control. These approaches are designed to either impede the transmission of vibration energy into the housing or reduce the effect of the dynamic mesh force excitation. Here, these concepts are analyzed to determine the levels of required actuation efforts and the corresponding driver electrical power requirements. Note that while the overall goal is to reduce the housing response, each concept attempts to control the vibrations at different structural points inside the gearbox system. Therefore, their control requirements may be inherently different. Details associated with each of these concepts are provided next.

3.1. Concept 1: inertial-based active gear actuator

The first approach uses three inertial actuators, which can be made of magnetostrictive or piezoelectric stacks, directly mounted tangentially onto the side of the gear body at equal angular intervals, as shown in Fig. 4. As the smart material expands and contracts at the selected excitation frequency, the acceleration of the inertial mass mounted on one end of the actuator will

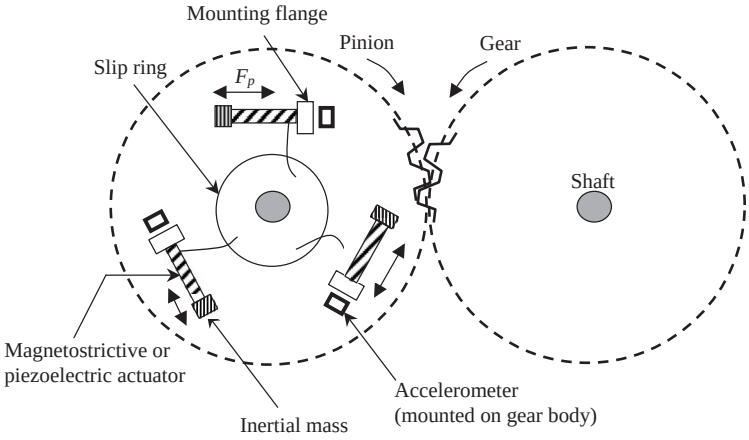

Fig. 4. Smart gear with inertial actuators (concept 1).

provide a reaction force that acts on the gear body. Due to the circumferential arrangement, these actuators can produce a net torque fluctuation as well as a translation force parallel to the mesh load line-of-action. The relative amount of these two actuation loads can be controlled by appropriately phasing the drivers. The net dynamic torque and force can then be applied in a controlled manner to reduce gear torsional and translational vibrations. Since this actuation concept directly acts near the excitation source, it is expected to be able to suppress vibrations transmitted into the shaft and bearings, and also reduce dynamic mesh force production. Additionally, the overall design includes three miniature accelerometers, located near the actuators, to measure gear vibrations and provide feedback signals to the controller.

To keep the actuation design as simple as possible, only the driven gear (or pinion) is treated. Since one of the purposes is to minimize the generation of dynamic mesh force, which involves lowering dynamic transmission error dictated by the relative motion at the mesh, it is only necessary to actuate one of the two gears. The disadvantage here is the lack of vibration transmissibility control through the shaft of the untreated gear. Note that a related design was used by Chen and Brennan [7] as indicated earlier. The fundamental difference is that the control object of Ref. [7] was the gear torsional vibration, while the goal in this work is to suppress the gear housing vibration.

Other considerations include the design of the fundamental resonant frequency of the actuator, which ideally needs to be near or less than the excitation frequency, and the fact that we have a set of rotating actuators requiring the use of slip rings. In the former issue, either an amplification mechanism, such as the displacement amplification or a series stiffness configuration may be needed to lower the first resonant frequency below the working frequency [19]. This is especially critical when a piezoelectric type actuator is selected since its resonant frequency is inherently high. In the latter problem, suitable slip rings with proper power ratings must be used to ensure sufficient supply of power to the rotating actuators. Of course, the slip rings are also needed for the accelerometer signals.

3.2. Concept 2: semi-active gear–shaft coupling

The second proposed concept is aimed at modifying the torsional vibration transmission path between the gear and shaft. In this set-up, the gear body and corresponding shaft are connected

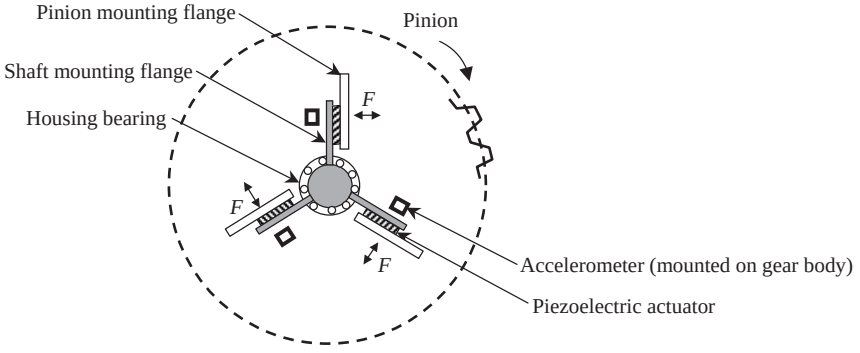

Fig. 5. Active control of gear–shaft torsional coupling (concept 2).

via several piezoelectric actuators, as shown in Fig. 5 for one set of gear–shaft coupling set-up. The piezoelectric actuators serve two purposes. They transmit the mean torque in the gear–shaft load path and simultaneously generate reactive dynamic forces to minimize transmitted perturbations. Like the first concept, slip rings are needed to provide input power to the actuators. Note that the translation force of the gear is transmitted via a rolling element bearing between the gear body and shaft.

This particular actuation concept is similar to the application of an active dynamic force directly on the shaft (the receiver) with a reaction against a gear body (the mass), as described in Ref. [4]. Therefore, the dynamic force required to isolate the torsional vibration transmitted from the gear into the shaft is inversely proportional to the excitation frequency. Accordingly, at relatively high frequency, only a small dynamic force is needed. However, when the frequency is lower, a large dynamic actuation force is required. Note that this scheme may also provide some level of passive torsional vibration isolation in the lower frequency range due to the semi-active nature of the structural design.

3.3. Concept 3: direct active bearing vibration control

Since most gear whine problems are the result of structure-borne vibration transmission from the geared rotor system through the bearings and into the housing, a natural path control scheme inside the gearbox is to set-up 'choke' points at the support bearings. One way to accomplish this is to use two pairs of piezoelectric stack actuators placed in two orthogonal radial directions between the bearing raceway and the housing support structure, as shown in Fig. 6. One pair of opposing actuators is oriented parallel to the gear mesh line-of-action, while the second pair is oriented perpendicular to the line-of-action. Note that although only one pair of actuators oriented parallel to tooth load line-of-action is needed theoretically, this double set configuration is recommended in practice to achieve a more robust ability to control general transverse plane motions of the shaft-bearing structure. This is especially useful when non-negligible transverse vibration orthogonal to the load line-of-action caused by misalignment and friction force excitation exists. In this work, the analyses of concepts 2 and 3 only incorporate the idealized single pair actuator case.

This specific actuation concept is designed to directly add active dynamic forces to the housing support structure by reacting against the bearing raceway, which may effectively suppress the

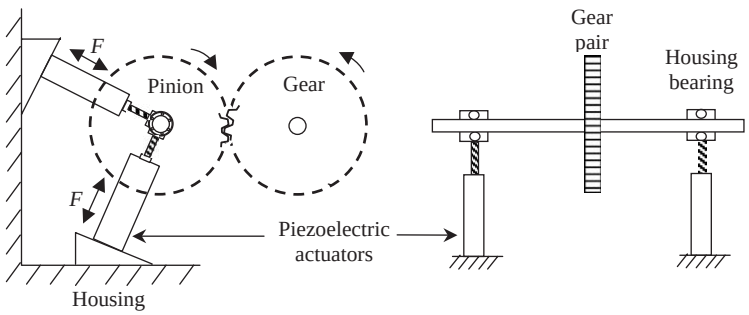

Fig. 6. Active control applied directly at the bearings (concept 3).

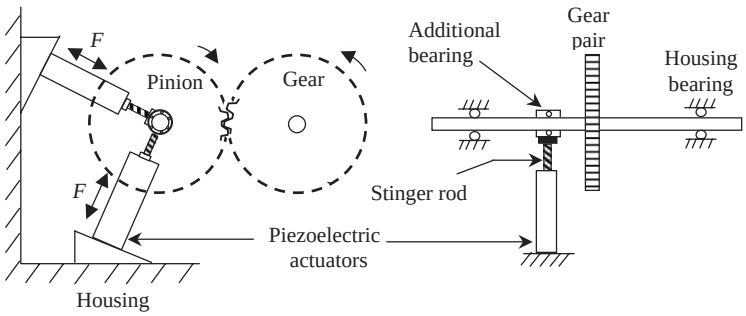

Fig. 7. Active shaft transverse vibration control (concept 4).

housing vibration. Unlike the previous two concepts, the actuators here are stationary. As a result, slip rings are not needed in this design. Nevertheless, the housing supports must be modified substantially to accommodate the actuators, which may not always be feasible.

3.4. Concept 4: active shaft transverse vibration control

In the final proposed concept, two pairs of actuators are attached to the rotating shaft using an additional set of bearing, as shown in Fig. 7. Unlike the third concept, here the actuators are acting against an additional, redundant bearing. Although the dynamic force is still being introduced between the shaft and housing, the added bearing component does not carry the required static load. Therefore, this bearing can accommodate a large range of motion. A similar idea was examined by Rebbechi et al. [6]. It is beyond the scope of this paper to discuss the optimum location of the actuation position relative to the gear pair. For the present analysis, it is assumed that the actuation position is located at one-third of the length from the gear position to the housing support location based on packaging considerations. Furthermore, due to the possible run-out and vibration deformation of the shaft, the actuators may see some lateral motions that may be harmful to the actuators. Hence, the set-up must be carefully designed such that the actuators are not directly connected to the bearing raceway. Instead, a thin stinger rod as shown in Fig. 7 is used. This stinger rod provides some degree of lateral flexibility, thereby reducing the potentially harmful lateral forces in the actuator.

4. Actuation dynamic forces

With the system model and the four actuation concepts defined, the required dynamic force for each concept to reduce housing vibrations can now be determined. In the active vibration control simulations involving actuation concepts 1, 3 and 4, the baseline dynamic FE model is used. In the case of actuation concept 2 on semi-active gear–shaft torsional coupling, the gear–shaft connection (that is rigid in the baseline FE model) is replaced by a lumped spring–damper element along the rotational co-ordinate, while all other parameters remain the same. The geared rotor system is assumed to be excited only by the gear transmission error under loaded conditions, which is typically on the order of 1–100 μm depending on manufacturing errors, tooth profiles,

elastic deformations and transferred loads [20]. In this study, it is assumed that the magnitude of the transmission error at the mesh frequency of excitation is nominally 10 μm. As depicted in Fig. 3, the transmission error excitation yields a pair of translational dynamic force and torque fluctuations acting on the gear and pinion. Hence, the excitation force vector **F** in Eq. (6) can be expressed as

$$\mathbf{F} = [0\cdots0 \quad \underset{\uparrow}{K_m} \quad 0 \quad \underset{\uparrow}{-K_m R_g} \quad 0\cdots0 \quad \underset{\uparrow}{-K_m} \quad 0 \quad \underset{\uparrow}{-K_m R_p} \quad 0\cdots0]^T e, \qquad \begin{matrix} & & u_{zg} & & \theta_{yg} & & u_{zp} & & \theta_{yp} \end{matrix} \tag{9}$$

where e is loaded transmission error represented mathematically as $10e^{i\omega_m t}$ μm that considers only the fundamental mesh harmonic, and u_{zg}, u_{zp}, θ_{yg} and θ_{yp} are the gear and pinion translation and rotation co-ordinates, respectively. Omitting the damping term, the dynamic mesh force can be formulated as [14]

$$F_{mesh} = K_m(u_{zg} - u_{zp} - R_g\theta_{yg} - R_p\theta_{yp} - e). \tag{10}$$

The predicted dynamic mesh force for the geared rotor system of interest (see Table 1 for actual design parameters) is shown in Fig. 8. The trend shows a general increase in F_{mesh} as frequency increases. This is due to the contribution from the fundamental mesh mode (out-of-phase rotation of the gear pair) at around 7 kHz (not shown in the figure) for this set of spur gears. It is also worthwhile to point out that the operating mesh frequencies and its first few harmonics are well below the fundamental gear pair resonance around 7 kHz. Thus, the non-linear type of response that typically associates with the gear mesh resonance can be safely neglected. This allows the analysis to be limited to the linear domain. Furthermore, the use of modal damping in the simulation permits the omission of explicit mesh damping term in Eq. (10).

The vibratory response of the gear housing due to a unit magnitude of dynamic force at the gear mesh co-ordinate can be calculated using the modal superposition-based transfer function theory given by Eq. (8). By scaling the equation linearly to reflect the total mesh force and summing the contributions from the resultant dynamic forces and torques on the gear and pinion, the net

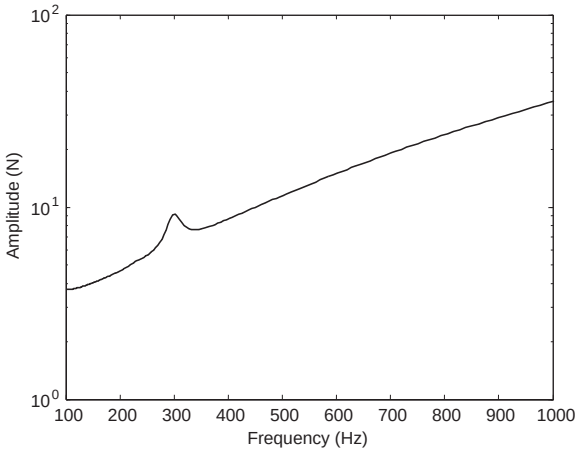

Fig. 8. Dynamic mesh force spectrum of the gear pair system of interest due to 10 μm of transmission error excitation.

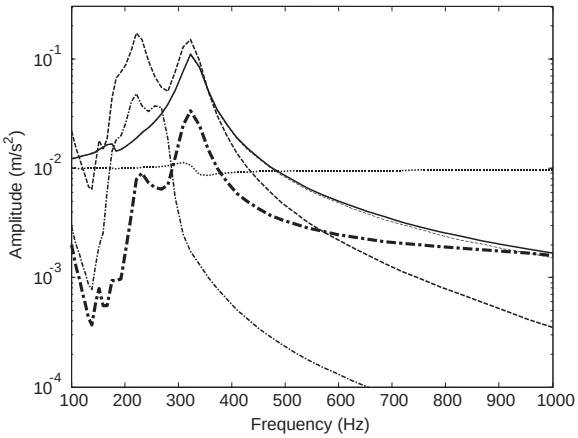

Fig. 9. Housing vibration spectrum due to unit force/torque input at various actuation positions compared to net response due to 10 μm of transmission error excitation (-·-·-): ——, shaft force actuation; · · · ·, bearing force actuation; - - -, gear force actuation; — — —, gear torque actuation; — · — ·, gear–shaft coupling force actuation.

displacement response of the housing (parallel to the load line-of-action vector) due to the specified transmission error excitation, $y_{h,TE}$, is given by

$$y_{h,TE} = \sum_{k=1}^{4} H_{hk} F_k = \sum_{i=1}^{N} \left[\frac{\phi_{hi}}{s^2 + 2\zeta_i \omega_i s + \omega_i^2} \sum_{k=1}^{4} \phi_{ki} F_k \right], \tag{11}$$

where F_k, $k = 1$–4, are the four non-zero forcing elements in Eq. (9). By taking the second time-derivative of displacement $y_{h,TE}$, the acceleration response of the housing is obtained, which is shown as the dashed-dotted curve in Fig. 9. The significance of the other curves in this figure will be discussed later.

As it is assumed that the geared rotor system is a linear time-invariant plant and the amplitude of gear transmission error excitation under load remains constant while the gears are actively controlled, the net response of the gear housing due to two separate forcing functions, i.e., the gear transmission error and the supplied dynamic actuation force, can be obtained algebraically. Note that the analysis remains general in spite of assuming constant amplitude transmission error excitation. This is because the linear time-invariant nature of the gearbox system allows one to scale the actuation force proportionally in the event that the amplitude of transmission error varies. The dynamic actuation force denoted by F_r is applied at the rth co-ordinate of the FE model. Depending on the application, F_r can be a force or a torque. Hence, the net housing response along the load line-of-action direction, y_h, due to the gear mesh excitation and the externally applied actuation force, is

$$y_h = y_{h,TE} + H_{hr} F_r. \tag{12}$$

Here, H_{hr} is the transfer function relating the rth actuation co-ordinate to the gear housing response co-ordinate, which is calculated using Eq. (8). In order to completely suppress the

housing vibration, we set $y_h = 0$ and solve for the required actuation force as

$$F_r = -y_{h,TE}/H_{hr}, \tag{13}$$

assuming that the system is controllable, i.e., H_{hr} is not singular at any frequency point of interest or not zero at the actuator location. Eq. (13) is in fact very general and can be employed to calculate the dynamic actuation force or torque at any co-ordinate to achieve a relative state of minimal housing vibration level. This theory is used next to predict the required actuation forces for the four concepts of interest.

First, consider the inertial-based active gear actuator system of Fig. 4. Suppose the three inertial actuators are excited in such a way that their net effect generates either a pure torque or pure translational force on the gear body in the θ_{yg} or u_{zg} co-ordinate, respectively. Recall that the actuators are mounted on the driven gear only. The housing vibration spectrum level due to a unit pure translation force or torque acting on the gear body is shown in Fig. 9, and respectively labeled as the gear force or torque actuation case. Note that this response is essentially the transfer function, expressed as $-\omega^2 H_{hr}$, relating the gearbox housing acceleration response and the actuation co-ordinate. From Fig. 9, two response peaks around 200–320 Hz can be observed for the pure torque actuation case. On the other hand, the pure force actuation curve has only one noticeable peak around 320 Hz. This difference occurs because of an out-of-phase torsion mode around 200 Hz that is not excited by the pure force actuation case. Using Eq. (13), the required net actuation efforts can be predicted as shown in Fig. 10. As expected from the response shown in Fig. 9, the required net actuation effort for the gear torque case given in Fig. 10 is relatively small at about 200 Hz. However, at other frequency points, the required net actuation effort for the pure torque case is much larger than that of pure translational force case. Notice that in order to compare the pure force and torque cases, the computed dynamic torque is transformed into an equivalent dynamic force by dividing the net torque with the gear base radius. This treatment of

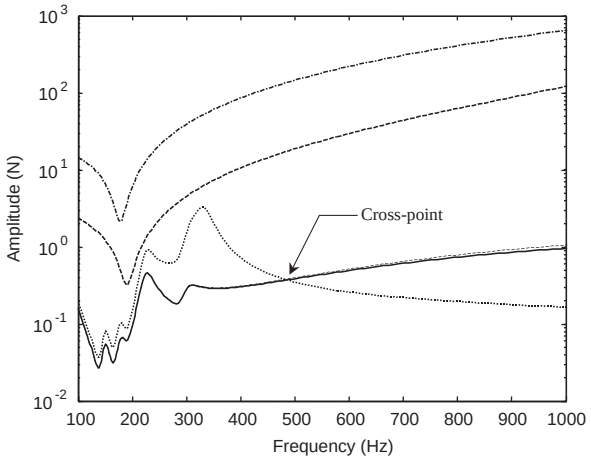

Fig. 10. Required dynamic actuation forces of the four active vibration control concepts to suppress housing vibrations due to 10 μm of transmission error excitation at the mesh frequency: ———, concept 1—pure torque actuation; - - -, concept 1—pure translation force actuation; — · — ·, concept 2; · · · ·, concept 3; ——, concept 4.

the torque is adopted from this point onwards such that it can be compared more directly with the force term.

In the second proposed concept on the use of semi-active gear–shaft coupling, it is again assumed that only the driven gear is treated. In this design, the actuators are configured to synthesize the internal dynamic torque acting between the gear and shaft. Hence, the instantaneous reaction torque on the gear is always out-of-phase with the torque acting on the shaft. The treatment of these reaction torques is in fact similar to the formulation of the effect of F_{mesh} in Eqs. (9) and (10). Based on this assumption, the net housing response due to this type of actuation can be determined using

$$y_{h,T} = \sum_{k=1}^{2} H_{hk} T_k = \sum_{i=1}^{N} \left[\frac{\phi_{hi}}{s^2 + 2\zeta_i \omega_i s + \omega_i^2} \sum_{k=1}^{2} \phi_{ki} T_k \right], \tag{14}$$

where $T_1 = -T_2$ are the actuation torque generated and the corresponding reaction torque. Furthermore, Eq. (13) can be applied to determine the required actuation torque by replacing $y_{h,TE}$ by $y_{h,T}$. Like the case of the inertial-based active gear vibration control concept, the required actuation torque can be transformed into an equivalent dynamic force. Its actuation force prediction is also given in Fig. 10 for comparison with the other actuation concepts. From the results, it appears that this method (concept 2) would require the largest actuation effort.

For the direct active bearing vibration control and active shaft transverse vibration control concepts, it is also assumed that only the driven gear–shaft is treated. For both concepts, Eq. (13) is again used to compute the required actuation force by setting the r-co-ordinate to the corresponding actuator position. The predictions of the housing response spectra due to the added unit actuation force, and also the actuation force required to completely suppress the transmission error generated housing vibration are shown with the results of the other concepts in Figs. 9 and 10, respectively. The housing vibration levels due to each one of these two unit actuation forces applied separately exceed the vibration amplitude due to the prescribed transmission error in all frequency range of interest except for the points around 300–400 Hz. In this narrow range, the housing response due to the added unit actuation force pertaining to concept 3 is lower. As a result, the required actuation forces for these two active control concepts are less than 1.0 N except around 300–400 Hz for the case of direct active bearing vibration control, as shown in Fig. 10. Also from these calculation results, it is clear that the actuation force of the third concept is the least for frequencies above 500 Hz. However, the actuation force of the active shaft transverse vibration approach (concept 4) is lower for frequencies below 500 Hz. The increased force in concept 3 in the lower frequency range is due to the two shaft bending modes that occur below 500 Hz, as seen in the transmission error generated housing response spectrum. These modes prevent the actuation force, which is applied directly to the bearing, from efficiently controlling vibration transmissibility. The simulation results also show that the actuation efforts for concepts 1 and 2, involving torsional co-ordinate control, are significantly higher across the entire frequency range of interest. This is due to the fact that these two concepts are more effective at controlling torsional motion only and not able to effectively impact transverse vibration. It may be noted that the net gear translation force (concept 1) is essentially identical to the actuation force spectrum of concept 4. This is because the actuation point of concept 4 is located very close to the gear body itself.

5. Electrical power requirements

Apart from the required actuation forces, the corresponding input electrical power is also of interest in the selection and design of the actuators and amplifiers. For the two active control methods involving torsional co-ordinates (concepts 1 and 2), the required dynamic torques are relatively large, and hence their input power needs will not be addressed explicitly here. Moreover, these actuators are rotating-type requiring slip rings, which further complicates their actual design and implementation. Therefore, the following analysis focuses mainly on the required input electrical power for the direct active bearing vibration control (concept 3) and active shaft transverse vibration control (concept 4), as they appear to be more efficient and easier to implement using typical piezoelectric stack type actuators.

It is generally accepted that a piezoelectric stack actuator can be modelled as a spring element of stiffness K_p when the working frequency ω of the actuator is far less than the first resonant frequency of the actuator [21–23]. Thus the mechanical impedance of the piezoelectric stack is $Z_p = K_p/\mathrm{i}\omega$. The block force F_b, defined as the maximum output force when the actuator is acting on a rigid structure with infinite impedance, is given by

$$F_b = K_p d_{33} V_3, \tag{15}$$

where d_{33} is the piezoelectric constant and V_3 is the external voltage applied along the axial direction of the stack. If the actuator is acting against a flexible structure, such as the bearing housing, the maximum possible output force F_r, which in this case is the same as the required actuation force, will decrease to yield

$$F_r = \frac{Z_{ext}}{Z_{ext} + Z_p} F_b, \tag{16}$$

where Z_{ext} is the external mechanical impedance at the r-co-ordinate given by

$$Z_{ext} = \frac{F_r}{\dot{x}_{rr}} = \sum_{i=1}^{N} \frac{s^2 + 2\zeta_i \omega_i s + \omega_i^2}{s\phi_{ri}^2}. \tag{17}$$

At the same time, the maximum possible stroke Δl for the actuator becomes $\Delta l = Z_p \Delta l_0/(Z_{ext} + Z_p)$, where Δl_0 is the nominal maximum stroke of the unconstrained actuator. On the other hand, the piezoelectric stack actuator can also be modelled as an electrical capacitor. Due to the inherent electrical–mechanical coupling, the dynamic electrical admittance Y is given by

$$Y = \frac{I_3}{V_3} = \mathrm{i}\omega C_0 \left[1 - \frac{k^2 Z_{ext}}{Z_{ext} + Z_p}\right], \tag{18}$$

where k^2 is the piezoelectric coupling coefficient, which is assumed to be 0.3, C_0 is the zero-stress electrical capacitance of the actuator, and I_3 is the applied current [23]. It is assumed here that C_0 is insensitive to temperature, in spite of the heat generated as the stack expands and contracts. Hence, the apparent power W_A output from the amplifier can be estimated as [23]

$$W_A = V_3^2 |Y|/2. \tag{19}$$

Using Eqs. (16)–(18) and the actuation force results, the applied voltage V_3 can be calculated. Eqs. (18) and (19) are subsequently used to determine the operating current I_3 and estimated

Table 2
Specification of actuator parameters (Model PSt1000/16/20 VS 25 by Piezomechanik GmbH [24])

Parameters	Numerical value (unit)
Operating voltage, V	0–1000 V
Maximum stroke, Δl_0	17 μm
Actuator length, L	35 mm
Actuator diameter, D	25 mm
Capacitance, C_0	150 nF
Stiffness, K_p	400 N/μm
Resonance, f_0	35 kHz

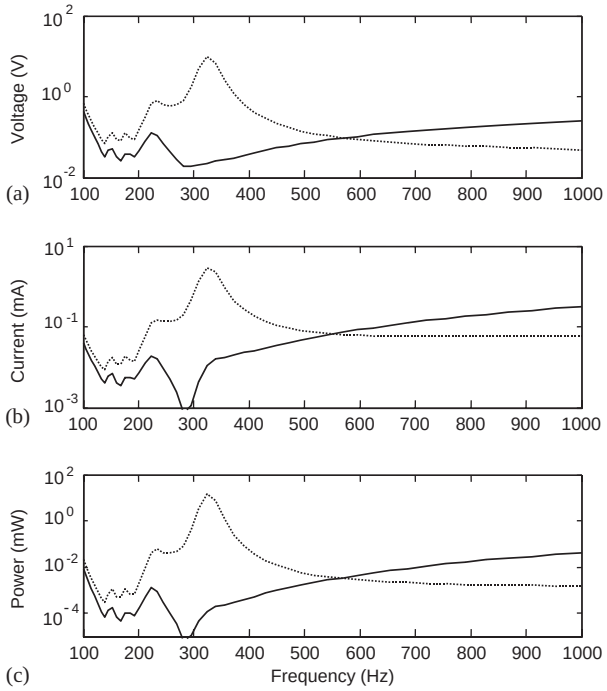

Fig. 11. (a) Input voltage, (b) operating current and (c) required electrical power for actuation concepts 3 (—) and 4 (· · ·).

power. To examine typical requirements, a specific high-voltage actuator was selected for the numerical study. The specifications for this actuator are listed in Table 2.

For the specific actuator of interest, the predicted input voltage, current and power needed to deliver the actuation force to suppress housing vibrations are shown in Fig. 11 for both direct active bearing vibration control (concept 3) and active shaft transverse vibration control (concept 4) approaches. Comparison of Figs. 10 and 11(a) indicates that even though the actuation forces for concepts 3 and 4 are relatively small below 200 Hz, the input voltages for this range are not very small compared to the values in the higher frequency range. The voltages are large because

the impedance of the external structure (the shaft or bearing) is quite small compared to that of the actuator, thereby limiting the output force F_r as indicated in Eq. (16). Comparison of Figs. 11(a) and (b) indicates that the input voltage and current for concept 4 are rather small near 280 Hz. The small levels obtained are the result of the close match between the impedances of the actuator and shaft. Hence, according to Eq. (18), the electrical admittance Y is small around this frequency. Due to the small level of input current near 280 Hz, the apparent power is small as well, as shown in Fig. 11(c). Note that these results can be useful in selecting a suitable amplifier to drive the actuator.

6. Sensitivity to measurement noise

To implement the above actuation method, it is convenient to choose the filtered-X LMS algorithm to design and adapt a controller that is essentially a finite impulse response (FIR) filter. This algorithm requires a reference signal $r(n)$ that must be highly correlated with the transmission error excitation signal $e(n)$. In this analysis, the gear mesh frequency signal along with a measured residual signal of the housing vibration $y_h(n)$ is utilized. However, these two signals are easily contaminated by measurement noises $m_1(n)$ and $m_2(n)$ as pointed out in the active vibration control diagram in Fig. 12. Hence, it is critical that the sensitivity of the proposed actuation methods to these two noise sources be known.

Suppose the adaptation of the controller is slow and the exact transfer function of the secondary path $H_{hr}(z)$, from the actuator output to the measured residual input signal, is known. The FIR weight $W(z)$ of the controller will then converge to an optimal value [25]:

$$W(z) = \frac{H_{hTE}(z)S_{re}(z)}{[S_{rr}(z) + S_{m_1m_1}(z)]H_{hr}(z)}, \tag{20}$$

where $S_{re}(z)$ is cross-power spectrum between $r(n)$ and $e(n)$, while $S_{rr}(z)$ and $S_{m_1m_1}(z)$ are the auto-power spectra of $r(n)$ and $m_1(n)$, respectively. Also, H_{hTE} is the transfer function relating the transmission error excitation to the housing vibration, which is also the primary path transfer function given by $y_{h,TE}/e$. Since the reference signal $r(n)$ is related to the excitation signal $e(n)$, the optimal solution of $W(z)$ in Eq. (20) is not exactly the same as those given in Refs. [25–27]. The

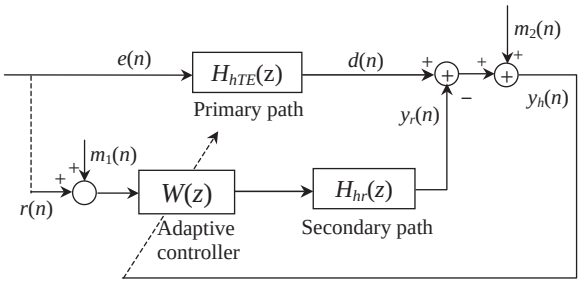

Fig. 12. Proposed active vibration control system.

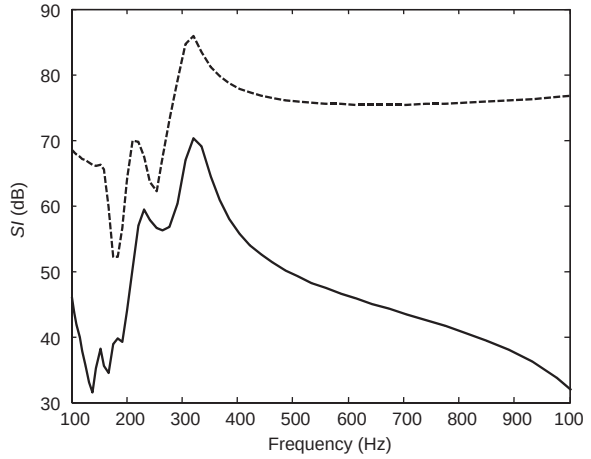

Fig. 13. Sensitivity indices of actuation concepts 1, 3 and 4 (——) and actuation concept 2 (– – –).

residual signal of the housing vibration is given by

$$S_{y_h y_h}(z) = S_{m_2 m_2}(z) + |H_{hTE}(z)|^2 \left(S_{ee} - \frac{|S_{re}(z)|^2}{S_{rr}(z) + S_{m_1 m_1}(z)} \right), \tag{21}$$

where $S_{ee}(z)$, $S_{m_2 m_2}(z)$ and $S_{y_h y_h}(z)$ are the auto-power spectra of $e(n)$, $m_2(n)$ and $y_h(n)$ respectively. Eq. (21) shows that if the power of the measurement noises $m_1(n)$ and $m_2(n)$, transmission error signal $e(n)$, and reference signal $r(n)$ are the same for the four actuation concepts, then the residual vibration signal of the gear housing will be mainly controlled by the primary path transfer function H_{hTE}. The first term in the right-hand side of Eq. (21) shows that the measurement noise $m_2(n)$ will remain in the housing vibration signal without any change. The second term shows that the housing vibration cannot be suppressed completely as long as some level of noise $m_1(n)$ is present. This is because the reference signal is directly affected by the adaptation of controller weight $W(z)$. From the above argument, we can conclude that the sensitivity to measurement noise is affected mainly by the primary path transfer function H_{hTE}. To quantify this further, a sensitivity index (SI) is defined as

$$SI = 20 \log(|H_{hTE}|). \tag{22}$$

Note that a higher sensitivity index implies a decrease in performance since the residual housing vibration level is greater. The calculated sensitivity indices for the four actuation concepts are shown in Fig. 13. The results reveal that the SI function of concept 2 is different and higher than the other three concepts across the entire frequency range of 100–1000 Hz. Therefore, this implies that concept 2 is the worst configuration among these four actuator concepts based on just this particular criterion. This conclusion is not too surprising as concept 2 is better suited to control purely torsional motion as opposed to the translational motion of the housing.

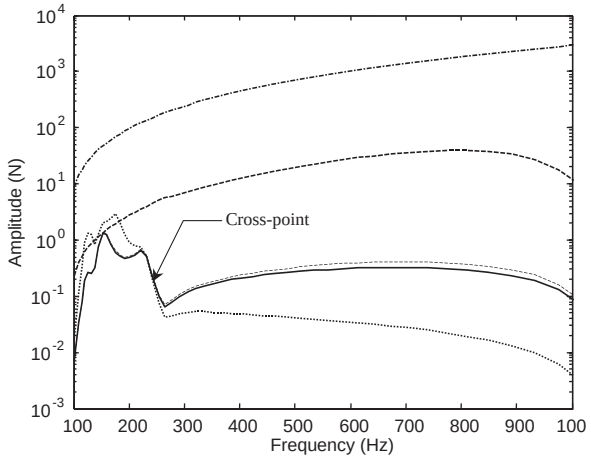

Fig. 14. Required dynamic actuation forces for the case of reduced 6.35 mm shaft diameter (baseline value is 9.5 mm): – – –, concept 1—pure torque actuation; - - -, concept 1—pure translation force actuation; – · – · , concept 2; · · · · , concept 3; ——, concept 4.

7. Parametric analysis

Even though the above numerical study was performed on a specific set of gearbox parameters, the theory is general and applicable to other types of geared rotor systems, as long as the corresponding FE model can be accurately constructed. To test the generalization of the above results, a select set of parametric studies is performed. Two cases of modifying the shaft diameter are studied. One involves reducing the shaft diameter from 9.5 to 6.35 mm, and another case uses a larger 12.7 mm diameter shaft. Furthermore, two cases of bearing stiffness variations are studied. For all of these cases, the required forces for concepts 1 and 2 related to torsional motion control are significantly higher than the others over the entire frequency range of interest, as shown in Fig. 14 for the case of the reduced 6.35 mm shaft diameter. Also, for all of the cases examined, the net gear translation force of concept 1 is almost the same as the actuation force of concept 4, which is similar to the baseline cases discussed earlier. Additionally, above a certain cross-point frequency, like the one in Fig. 10, the actuation force of concept 3 is observed to be the smallest. Below this frequency, the actuation force of concept 4 is the smallest. For the two cases involving a modification in bearing stiffness, this cross-point frequency is not affected because the modes dominated by the bearing stiffness are quite high. The cross-point frequency is mainly dependent on the diameter of shaft. Therefore, in the smaller shaft diameter case, which implies a more flexible shaft, the cross-point frequency is lower.

8. Conclusions

The relative performance of four proposed actuation concepts designed to apply dynamic loads to the internal gearbox components in order to suppress housing vibration is examined in this research. The analysis includes the formulation of a suitable gearbox model for use in determining

the actuation force required in each concept. The corresponding driver voltage, current, and power for the two most promising concepts are also calculated, along with the sensitivities of all four approaches to measurement noise. Based on the numerical simulation results obtained, the dynamic actuation forces for the two active control concepts involving rotational co-ordinate, which are the inertial-based active gear actuator and gear–shaft torsional coupling, are found to be very large compared to the other concepts applying only translational actuation load. Furthermore, the gear–shaft torsional coupling case depicts the highest sensitivity to measurement noise. The direct active bearing vibration control approach requires the smallest dynamic actuation force above 500 Hz for the particular gearbox system considered in this study. However, below 500 Hz this approach needs a relatively large actuation force and correspondingly high input current, voltage and power. On the other hand, the active shaft transverse vibration control approach (concept 4) that is determined to be the best compromise requires the smallest dynamic force below 500 Hz and fairly reasonable parameters in the higher frequency range. Another advantage of concept 4 is the ease of implementation in a practical setting, since slip ring equipment is not used and no major structural modification is required. The outcome of this study is currently being applied to design a complete active control system using piezoelectric stack actuators for suppressing gear vibration and ultimately gear whine. Furthermore, while the gear housing vibration is targeted for control in this work, it may also be interesting to compare several different other control goals, such as the gear whine noise and dynamic mesh force. Such analysis will be addressed in future studies.

Acknowledgements

The material is based upon work supported by the US Army Research Laboratory and the US Army Research Office under contract/grant DAAD19-00-1-0158 (Project No. P-40942-EG-DPS). The ARO technical monitor is Dr. Gary Anderson.

References

[1] Y.S. Lee, S.J. Elliott, Active position control of a flexible smart beam using internal model control, Journal of Sound and Vibration 242 (5) (2001) 767–791.
[2] C.H. Park, A. Baz, Vibration control of bending modes of plates using active constrained layer damping, Journal of Sound and Vibration 227 (4) (1999) 711–734.
[3] S. Ikai, K. Ohsawa, K. Nagaya, H. Kashimoto, Electromagnetic actuator and stacked piezoelectric sensors for controlling vibrations of a motor on a flexible structure, Journal of Sound and Vibration 231 (2) (2000) 393–409.
[4] C.R. Fuller, S.J. Elliott, P.A. Nelson, Active Control of Vibration, Academic Press Inc, New York, 1996.
[5] A. Kahraman, R. Singh, Non-linear dynamics of a spur gear pair, Journal of Sound and Vibration 142 (1) (1990) 49–75.
[6] B. Rebbechi, C. Howard, C. Hansen, Active control of gearbox vibration, Proceedings of the Active Control of Sound, Vibration Conference, Fort Lauderdale, 1999, pp. 295–304.
[7] M.H. Chen, M.J. Brennan, Active control of gear vibration using specially configured sensors and actuators, Smart Materials and Structures 9 (3) (2000) 342–350.

[8] R. Maier, M. Pucher, W. Gembler, Helicopter interior noise reduction by active vibration isolation with smart gearbox struts, Proceedings of the Active Control of Sound and Vibration Conference, Fort Lauderdale, 1999, pp. 189–198.
[9] T.J. Sutton, S.J. Elliott, M.J. Brennan, Active isolation of multiple structure waves on a helicopter gearbox support strut, Journal of Sound and Vibration 205 (1) (1997) 81–101.
[10] I. Pelinescu, B. Balachandran, Analytical and experimental investigations into active control of wave transmission through gearbox struts, Smart Structures and Materials 2000: Smart Structures and Integrated Systems 3985 (2000) 76–85.
[11] S.S. Rao, The Finite Element Method in Engineering, 3rd Edition, Butterworth-Heinemann, Boston, MA, 1999.
[12] W.A. Tuplin, Gear tooth stresses at high speed, Proceedings of the Institution of Mechanical Engineers 16 (1950) 162–167.
[13] H.N. Ozguven, D.R. Houser, Mathematical models used in gear dynamics—a review, Journal of Sound and Vibration 121 (3) (1988) 383–411.
[14] H.N. Ozguven, D.R. Houser, Dynamic analysis of high speed gears by using loaded static transmission error, Journal of Sound and Vibration 125 (1) (1988) 71–83.
[15] F. Cricenti, C.H. Lang, D. Paradiso, Development of an analytical model for the static and dynamic transmission error calculation: validation on a single vehicle gear vibration test bench, Proceedings of the ASME Eighth International Power Transmission and Gearing Conference, Baltimore, DETC2000/PTG-14426, 2000.
[16] D.R. Houser, R. Singh, Gear Noise Short Course Notes, Ohio State University, Columbus, 2002.
[17] T.C. Lim, R. Singh, Vibration transmission through rolling element bearings, Part III: geared rotor system studies, Journal of Sound and Vibration 151 (1) (1991) 31–54.
[18] H.N. Ozguven, A non-linear mathematical model for dynamic analysis of spur gears including shaft and bearing dynamics, Journal of Sound and Vibration 145 (2) (1991) 239–260.
[19] J. Dosch, G. Lesieutre, G. Koopmann, C. Davis, Inertial piezoceramic actuators for smart structures, Proceedings of SPIE, Smart Structures and Materials: Industrial and Commercial Applications of Smart Structures Technologies 2447 (1995) 14–25.
[20] J.D. Smith, Gear Noise and Vibration, Marcel Dekker, New York, 1999.
[21] C. Liang, F. Sun, C.A. Rogers, Electro-mechanical impedance modeling of active material systems, Smart Materials and Structures 5 (2) (1996) 171–186.
[22] E. Flint, C. Liang, C.A. Rogers, Electromechanical analysis of piezoelectric stack active member power consumption, Journal of Intelligent Material Systems and Structures 6 (1) (1995) 117–124.
[23] S. Zhou, C. Liang, C.A. Rogers, Integration and design of piezoceramic elements in intelligent structures, Journal of Intelligent Material Systems and Structures 6 (6) (1995) 733–743.
[24] Piezomechanik GmbH, Piezoelectrical and Electrostrictive Stack Actuator Catalog, Piezomechanik GmbH, Munich, 2001.
[25] P.A. Nelson, S.J. Elliott, Active Control of Sound, Academic Press, London, 1992.
[26] B. Widrow, S.D. Stearns, Adaptive Signal Processing, Prentice-Hall, New Jersey, 1985.
[27] S.M. Kuo, D.R. Morgan, Active noise control: a tutorial review, Proceedings of the IEEE 87 (6) (1999) 943–973.